
Electronic Supplementary Material

Phase Transition of Metal–Organic Frameworks for Regulating Fluorescent Properties of Dyes

Ziyue Qin[1], Zhen Ren[1], Cheng Chen[1], Liwei Liu[2], Ning Ji[1], Yanhua Zhao[3], Baoli Zha[1], Yu Fu[2], Yu Shen[1] and Fengwei Huo[1]**

1. Key Laboratory of Flexible Electronics (KLOFE) and Institute of Advanced Materials (IAM), Nanjing Tech University (Nanjing Tech), Nanjing 211816, China

2. College of Sciences, Northeastern University (NEU), 11 Wenhua Road, Shenyang 100819, China

3. Shaanxi Institute of Flexible Electronics (SIFE), Northwestern Polytechnical University (NPU), 127 West Youyi Road, Xi'an 710072, China

Corrsponding Authors

iamfwhuo@njtech.edu.cn; iamyshen@njtech.edu.cn

Supplementary Methods

Experimental materials

All reagents were purchased commercially and used without external treatment. Zinc oxide (>99.0%), 2-methylimidazole (2-MeIm, 99%), and Basolite Z1200® (produced by BASF) were purchased from Sigma Aldrich. MIL-53 was purchased from HWRK. Rhodamine B (RhB) was purchased from Acros Organics, Fluorescein isothiocyanate (FITC) and Rhodamine 6G (R6G) were purchased by Aladdin and coronene was obtained from Macklin. MeOH, EtOH, dimethyl sulfoxide (DMSO), and dichloromethane (DCM) were purchased from Shanghai Titan Scientific Co.,Ltd.

Tablet Machine (T69YP-15A) was produced by Tianjin Keqi High&New Technology Corporation. Powder XRD patterns were recorded with with Rigaku SmartLab using Cu Kα radiation (λ = 1.5406 Å). Morphological features were studied using field emission scanning electron microscope (FESEM, JEOL JSM-7800F). UV-vis spectra were recorded on a Shimadzu UV-2501 spectrophotometer. The loadings of dyes were detected by UV-vis according to standard curves of dyes. Nitrogen sorption studies were performed in a Micromeritics ASAP 2460 adsorption apparatus at 77 K up to 1 bar. The pore textural properties including specific Langmuir and BET surface area, pore volume, and pore size were obtained by analyzing nitrogen adsorption and desorption isotherms with Micromeritics ASAP 2460 built-in software. All fluorescent images were acquired on Zeiss LSM880 NLO (2 + 1 with BIG) Confocal Microscope System. The fluorescence spectra for RhB were recorded from 520-800 nm upon exciting at 500 nm.[1] The excitation spectra were recorded from 300-570 nm when monitoring the fluorescence emission at 590-604 nm. Steady-state fluorescence spectra were measured by Hitachi F-4600. 500-long pass filter was used to minimize the scattered excitation light. The photoluminescence spectra and emission lifetime were obtained on a fluorescence spectrophotometer (Edinburgh FLS980) equipped with a 500 nm pulsed laser (YLS Supercontinuum Source) and a 375 nm optical laser (EPL-375, Edinburgh Instrument)[2]. The photoluminescence quantum yields of the solid samples were collected on a FLS980 spectrometer equipped with an integrating sphere with $BaSO_4$ as the reference. The decay curves are exactly fit by the following equation:

$$I(t) = \sum A_i e^{-t/\tau i}$$

where A_i is the preexponential factor for the lifetime τ_i. The average lifetime of fluorescence is calculated by $\tau = \sum A_i \tau_i$.

Raman spectroscopy was carried out using a WITEC alpha300M+ R instrument with a laser wavelength of 488 nm according to references.[3,4] All the other reagents were purchased from Sigma-Aldrich and used without further purification.

Methods

Preparation of RhB@ZIF-8 by PISA. 5 mg RhB and 95 mg ZIF-8 were mixed thoroughly and ultrasound in 5 mL MeOH. Then the samples were dried by rotary evaporator and kept in dried in 120 °C oven overnight. 20 mg of RhB/ZIF-8 were pressed via a T69YP-15A tablet machine. The powders were subjected to average pressures of 1364 MPa (9-ton, 13 mm diameter pellet die) for 5 min. RhB@ZIF-8 was prepared by exposing to MeOH at 50 °C for 0 h, 2 h, 4 h, 6 h, 24 h. The mixers were washed with MeOH for more than 10 times until the supernatants were colorless. After washing, the samples were dried at 50 °C for further use. The loadings of RhB in ZIF-8 were determined by the standard curve of RhB in MeOH (HCl) solvents after dissolving RhB@ZIF-8 in MeOH (HCl) solvents. To make the whole preparation process simpler, the 5 mg RhB and 95 mg ZIF-8 were mixed and ground thoroughly, then use PISA strategy to prepare RhB@ZIF-8. Similar methods can also be used to encapsulate other dyes such as FITC or coronene.

Photoluminescence Quenching of $RhB_{0.21}$@ZIF-8. The obtained $RhB_{0.21}$@ZIF-8 was transferred into 1 mL ethanol. Then, after adding 0.5 mL of the quenchers (5-(Bromomethyl)undecane, iodomethane), the time-dependent fluorescent intensity of $RhB_{0.21}$@ZIF-8 was tested by using fluorescence spectrometer. For control experiments, $RhB_{0.21}$@ZIF-8 was replaced by RhB or RhB/ZIF-8 mixers (the concentrations of RhB in EtOH were kept to 2 μg mL^{-1}).

Preparation of screen-printing patterns. 100 μL of the aloe vera gel and 5 mg $RhB_{0.21}$@ZIF-8 or $corenene_{3.65}$@ZIF-8 were mixed and painted with a squeegee onto a screen (2 cm × 0.8 cm), on which a transparent, pre-designed image was laid afterwards. After completely drying and hardening, the screen was laid over a filter paper and an ink containing $RhB_{0.21}$@ZIF-8 and $corenene_{3.65}$@ZIF-8 was printed onto the screen to generate a painting.

Preparation of RhB@ZIF-8 by ball-milling.[5] ZnO (40mg,0.491mmol), 2-methylimidazole (80.70mg, 0.982mmol), and RhB (5mg, 15 wt%) were placed into a plastic jar with three quartz balls (7mm). The mixture was neatly ground for 10 min at 30 Hz using IST-500 mixer mill, followed by further milling for 45 min by the addition of EtOH (45 μL) and 6 mg of NH_4Cl.The resulting compound was washed first with EtOH and then with toluene, filtered, and air-dried. The mixers were washed with MeOH for more than 10 times after grinding the pellets into powders. After washing, the samples were dried at 50 °C for further use. The loadings of RhB in RhB@ZIF-8 were determined by the standard curve of RhB/MeOH (HCl) solvents. The complete encapsulation of RhB cannot be achieved by in-situ ball milling (loading of RhB@ZIF-8 prepared by ball-milling was 0.46 wt%, the highest theoretical loading is 5 wt%).

Simplification of the method for preparation of RhB@ZIF-8. To simplify our methods, the effects of different treatment methods in the early stage on the luminescence properties and packaging amount of RhB/ZIF-8 material were explored. Solution phase mixing and rotary evaporation treatment were replaced by solid phase grinding, RhB/ZIF-8 obtained after 0 h and 24 h solution aging showed similar fluorescence emission and packaging amount compared to solution phase premixing, which indicates that RhB/ZIF-8 solid solvent can be prepared directly by solid-phase grinding.

5 mg RhB and 95 mg activated ZIF-8 were mixed and ground thoroughly. 20 mg of RhB/ZIF-8 were pressed via a T69YP-15A tablet machine. The dry powders were subjected to average pressures of 1364 MPa (9-ton, 13 mm diameter pellet die) for 5 min. RhB@ZIF-8 was prepared by exposing to MeOH at 50 °C for 0 h, 24 h. The

mixers were washed with MeOH for more than 10 times after grinding the pellets into powders. After washing, the samples were dried at 50 °C for further use. The loadings of RhB in RhB@ZIF-8 were determined by the standard curve of RhB/MeOH (HCl) solvents.

Photoluminescence Quenching of $\mathbf{RhB_{0.21}}$@ZIF-8. The obtained $RhB_{0.2}$@ZIF-8 (or RhB or ZIF-8 with RhB) were transferred into ethanol (1 mL). Then, after adding 5-(Bromomethyl) undecane and iodomethane (0.53 g, 2.1 mmol) or iodomethane (1.14 g, 8.0 mmol), the time-dependent fluorescent intensity of $RhB_{0.21}$@ZIF-8 was tested by using fluorescence spectrometer. For all experiments, the concentrations of RhB in EtOH were kept to 2 μg mL^{-1}.

Preparation of other dyes@ZIF-8 by PISA. 1 mg FITC or coronene and 19 mg activated ZIF-8 were mixed and ground thoroughly. Then the dyes/ZIF-8 mixers were pressed via a T69YP-15A tablet machine. The dry powders were subjected to average pressures of 1364 MPa (9-ton, 13 mm diameter pellet die) for 5 min. Dyes@ZIF-8 was prepared by exposing to MeOH at 50 °C for 0 h, 24 h. The mixers were washed with MeOH for more than 10 times after grinding the pellets into powders. After washing, the samples were dried at 50 °C for further use. The loadings of dyes in dyes@ZIF-8 were determined by the standard curve.

Table S1 Comparison of the loadings of dyes in ZIF-8 and other MOFs, the synthetic methods include in situ encapsulation, post synthetic methods (PSM), post solvents exchange and pressure-induced-stimulated-aging process.

Materials	Loading (wt%)	Methods	References
RhB@ZIF-8	0.0803	In situ encapsulation	6
RhB@Al-DBA	0.019	PSM	7
RhB@bio-MOF-1	60.14	PSM	8
Coronene@ZIF-8	1.46	In situ encapsulation	9
RhB@ZIF-8	**1.02**	**PISA**	**this work**
Coronene@ZIF-8	**3.65**	**PISA**	**this work**

Table S2 Fluorescence lifetime of RhB in MeOH, solid RhB and inside of ZIF-8 pores of RhB_n@ZIF-8 samples with increasing loading of RhB.

Samples	Fluorescence Lifetime (ns)	χ^2
Solid RhB	0.5	0.419
$RhB_{0.21}$@ZIF-8	2.4	0.920
$RhB_{0.62}$@ZIF-8	1.8	0.788
$RhB_{0.74}$@ZIF-8	1.8	1.331
$RhB_{0.90}$@ZIF-8	1.7	0.861
$RhB_{1.02}$@ZIF-8	1.7	0.841

Table S3 Comparison of the loadings of RhB in ZIF-8 and other photophysical properties of RhB loaded in other materials.

Materials	Loading (wt%)	Fluorescence Lifetime (ns)	Quantum yield (%)	References
RhB@ZIF-8	0.0803	-	23.2	6
RhB@Al-DBA	0.019	1.8/5.3	12	7
RhB@ZIF-8	-	4.07	-	10
MCM-Rh B	-	0.45/2.89	-	11
Phen-MCM-Rh B	-	0.42/2.80	-	11
RhB@ZIF-8	**0.21**	**2.4**	**20.3**	**this work**
RhB@ZIF-8	**1.02**	**1.7**	**9.0**	**this work**

Table S4 Fluorescence lifetime of solid FITC and FITC$_n$@ZIF-8 samples.

Samples	Fluorescence Lifetime (ns)	χ^2
Solid FITC	0.6	1.117
FITC$_{0.25}$@ZIF-8	2.0	0.886
FITC$_{1.19}$@ZIF-8	2.0	1.076

Table S5 The fluorescence lifetime of solid coronene and coronene$_n$@ZIF-8.

Samples	Fluorescence Lifetime (ns)	χ^2
Solid coronene	6.6	0.948
Coronene$_{2.37}$@ZIF-8	8.4	0.886
Coronene$_{3.65}$@ZIF-8	7.6	1.243

Table S6 The quantum yield of fluorescence for solid FITC and solid coronene.

Sample	Quantum Yield
Solid FITC	8.1%
Solid Coronene	4.1%

Table S7 The fluorescence lifetimes of solid RhB, and RhB/MIL-53 after aging in MeOH for different time.

Samples	Fluorescence Lifetime (ns)
Solid RhB	0.5
4 h recovered RhB/MIL-53	1.5
24 h recovered RhB/MIL-53	1.6

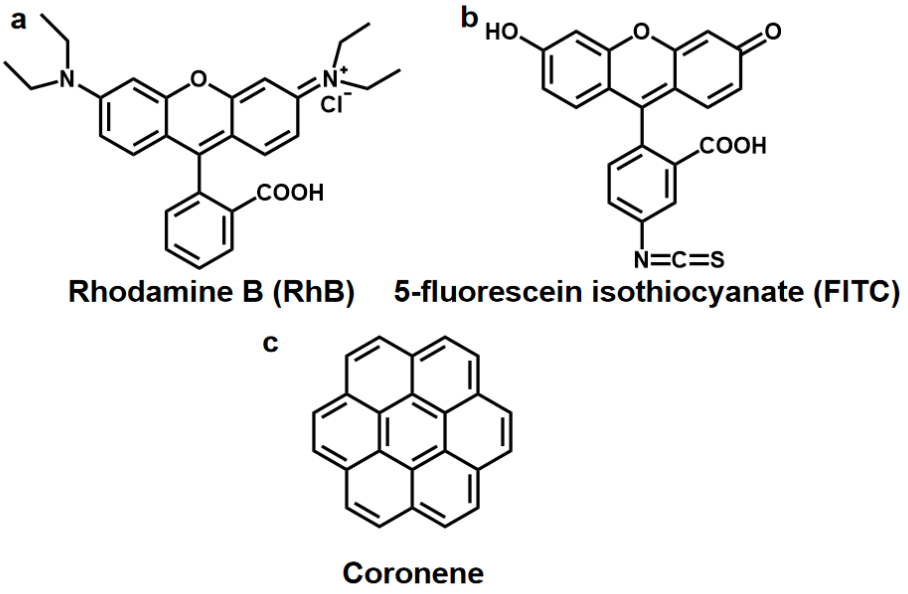

Fig. S1 The molecular structure of different dyes. (a) RhB; (b) FITC; (c) coronene.

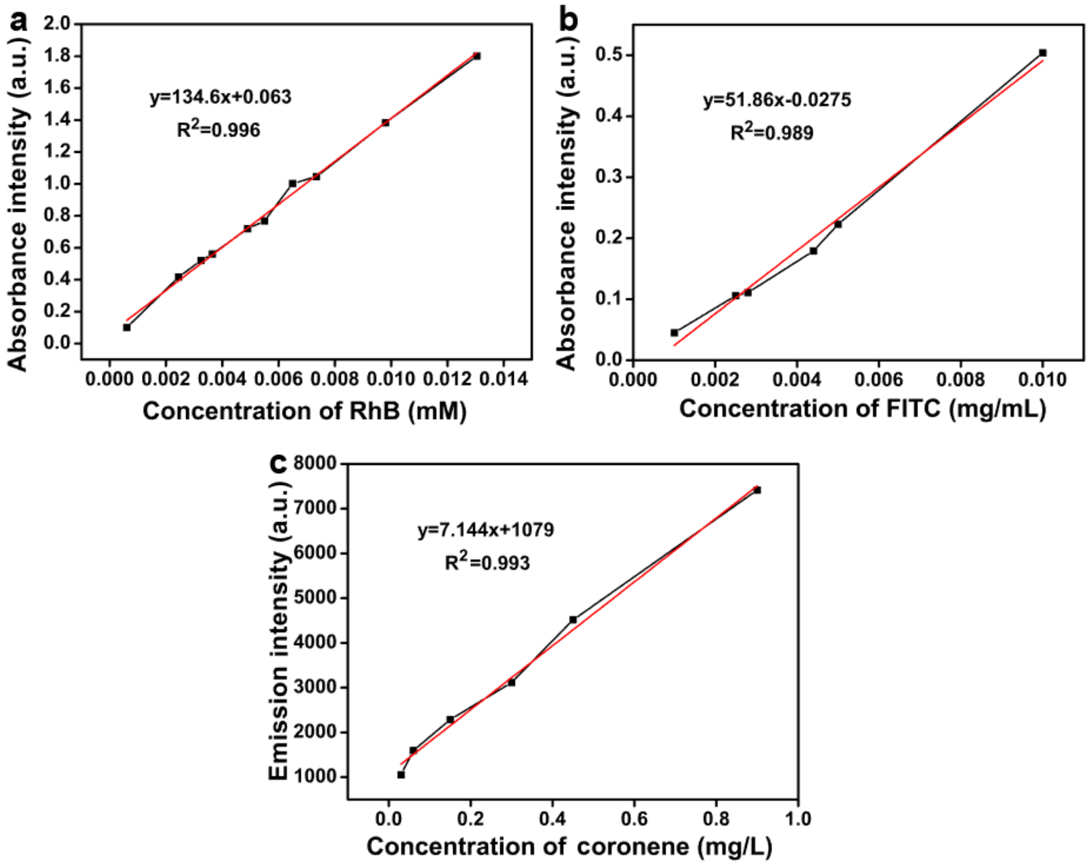

Fig. S2 (a) Standard curves of the dyes for the determination of concentration of dyes in ZIF-8. RhB (detected absorption at 553 nm); (b) FITC (detected absorption at 440 nm) (c) coronene (detected emission at 475 nm).

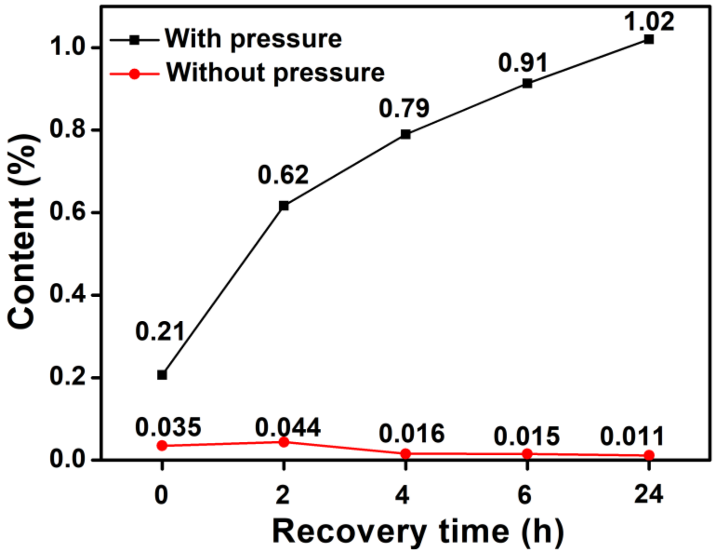

Fig. S3 Comparisons of the loadings of RhB in ZIF-8 under the treatment of pressure or without pressure aging or washing in organic solvents.

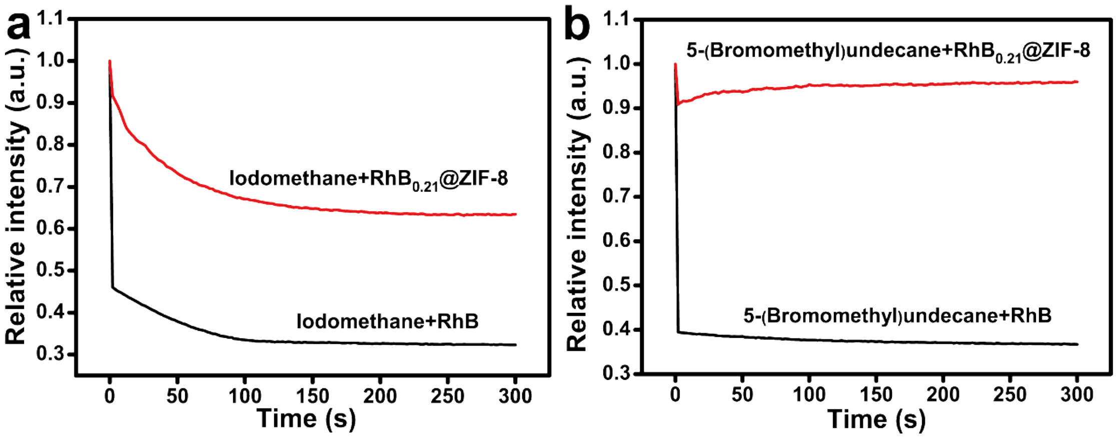

Fig. S4 (a) Normalized photoluminescence intensity of $RhB_{0.21}$@ZIF-8 and RhB versus time after the addition of small quencher (iodomethane) or large quencher (5-(bromomethyl)undecane). (b) Normalized photoluminescence intensity of $RhB_{0.21}$@ZIF-8 and RhB versus time after the addition of large quencher (5-(bromomethyl)undecane).

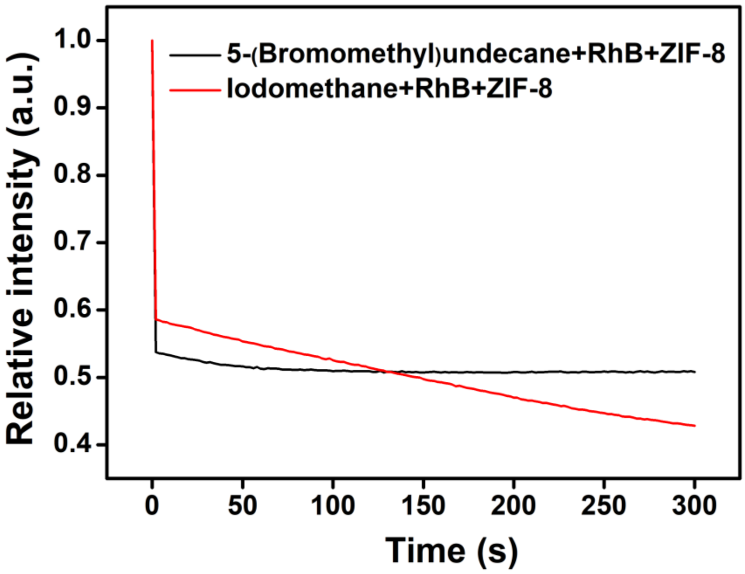

Fig. S5 Normalized photoluminescence intensity of RhB with ZIF-8 versus time after the addition of small quencher (iodomethane) or large quencher (5-(bromomethyl)undecane).

Before quenching tests, ZIF-8 with same amount was added to RhB in EtOH with ultrasound. Only 51% and 43% of emission intensity can be maintained under the treatment of larger quenchers or small quenchers, respectively.

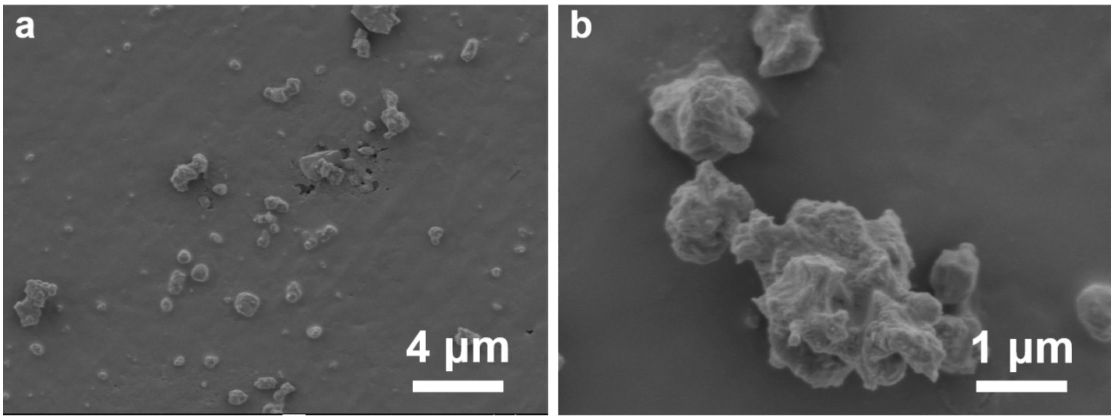

Fig. S6 SEM images of pressed RhB/ZIF-8 under 1364 MPa.

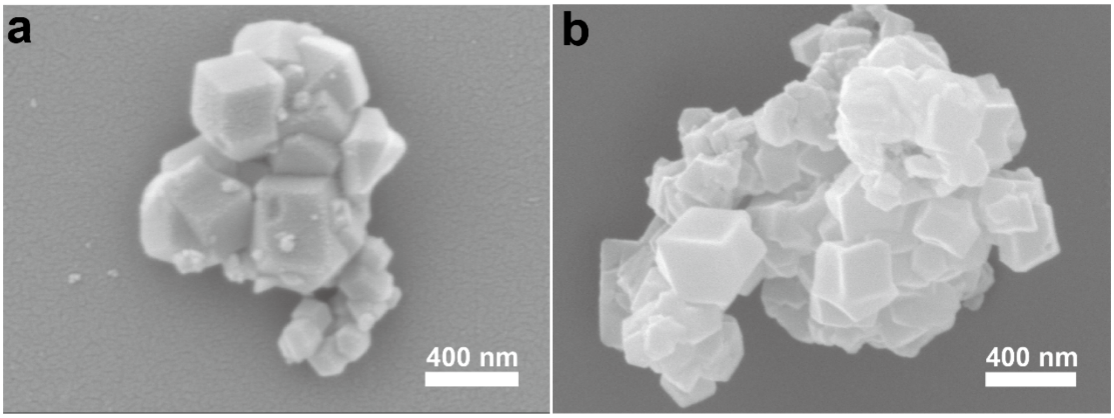

Fig. S7 (a) SEM image of commercial ZIF-8; (b) $RhB_{0.21}$@ZIF-8 after methanol recovery.

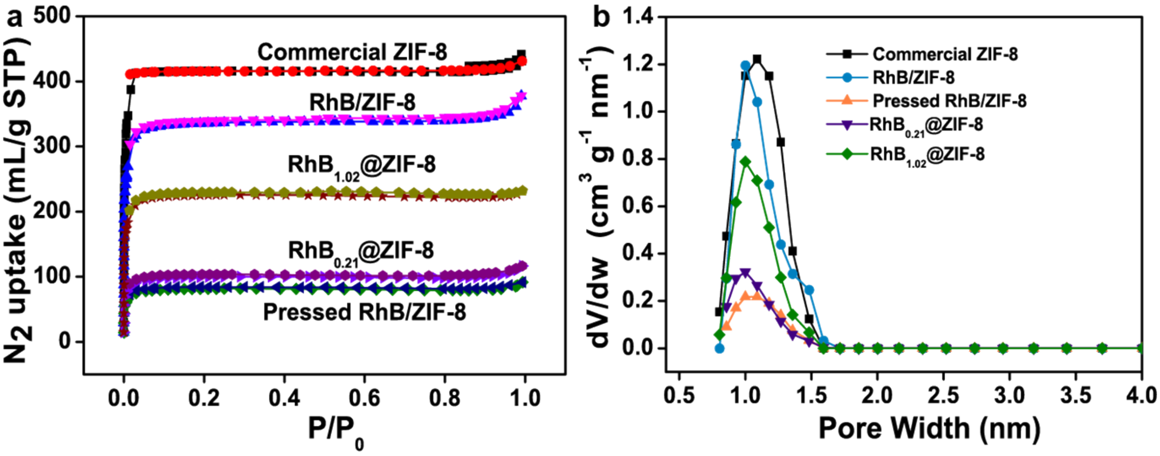

Fig. S8 (a) N_2 adsorption-desorption isotherm curves and (b) Pore analysis of commercial ZIF-8, RhB/ZIF-8, $RhB_{1.02}$@ZIF-8, $RhB_{0.21}$@ZIF-8, RhB/ZIF-8 under pressure.

It is found that RhB and ZIF-8 after mixing, the Brunauer-Emmett-Teller (BET) specific surface area decreased from 1847.6 $m^2 \cdot g^{-1}$ to 1419.1 $m^2 \cdot g^{-1}$. The specific surface area of RhB/ZIF-8 after high pressure treatment directly decreased to 328.2 m^2 g^{-1}, which proved the amorphization of ZIF-8. Moreover, due to pore collapse, the amorphous ZIF-8 lost 77% porosity, the porosity also decreased from 1 $cm^3 \cdot g^{-1} \cdot nm^{-1}$ to 0.212 $cm^3 \cdot g^{-1} \cdot nm^{-1}$. The above results confirmed that most of the ZIF-8 in RhB/ZIF-8 with a pressure of 1364 MPa had become amorphous. From N_2 sorption experiments, the specific surface area of direct cleaning also increased from 328.1 $m^2 \cdot g^{-1}$ to 396.1 $m^2 \cdot g^{-1}$, and the porosity increased from 0.212 $cm^3 \cdot g^{-1} \cdot nm^{-1}$ to 0.32 $cm^3 \cdot g^{-1} \cdot nm^{-1}$, indicating that partially amorphous ZIF-8 has changed to crystalline ZIF-8 during methanol washing. After 24 h recovery, the specific surface area of RhB/ZIF-8 was changed after washing. It is 915.8 $m^2 \cdot g^{-1}$, equivalent to 65% before recovery, which indicates that RhB/ZIF-8 under pressure is partially amorphous ZIF-8 transformed into partially crystalline ZIF-8 under methanol solvent treatment.

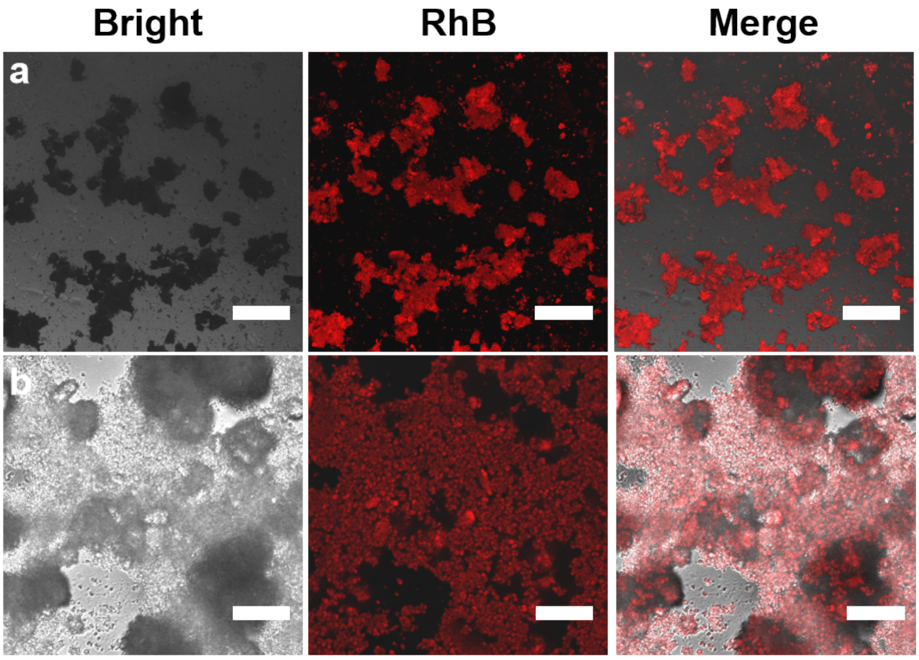

Fig. S9 Laser confocal fluorescence microscopy imaging of the $RhB_{0.21}$@ZIF-8 (scale bar of a: 25 μm, scale bar of b: 157 μm).

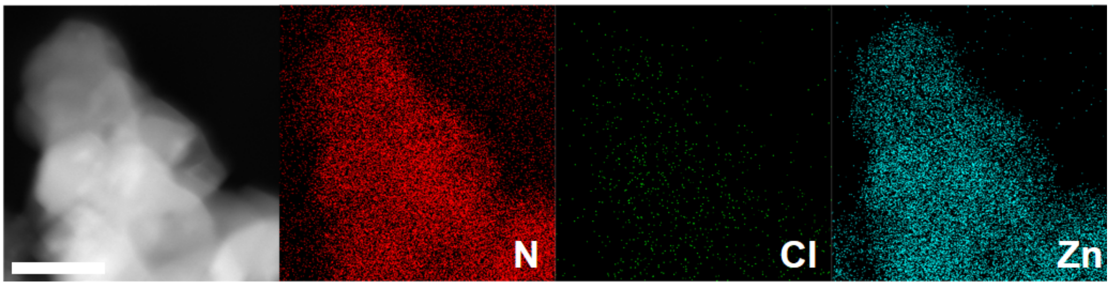

Fig. S10 EDS mapping of $RhB_{0.21}$@ZIF-8 (scale bar: 250 nm), the element of Cl from RhB.

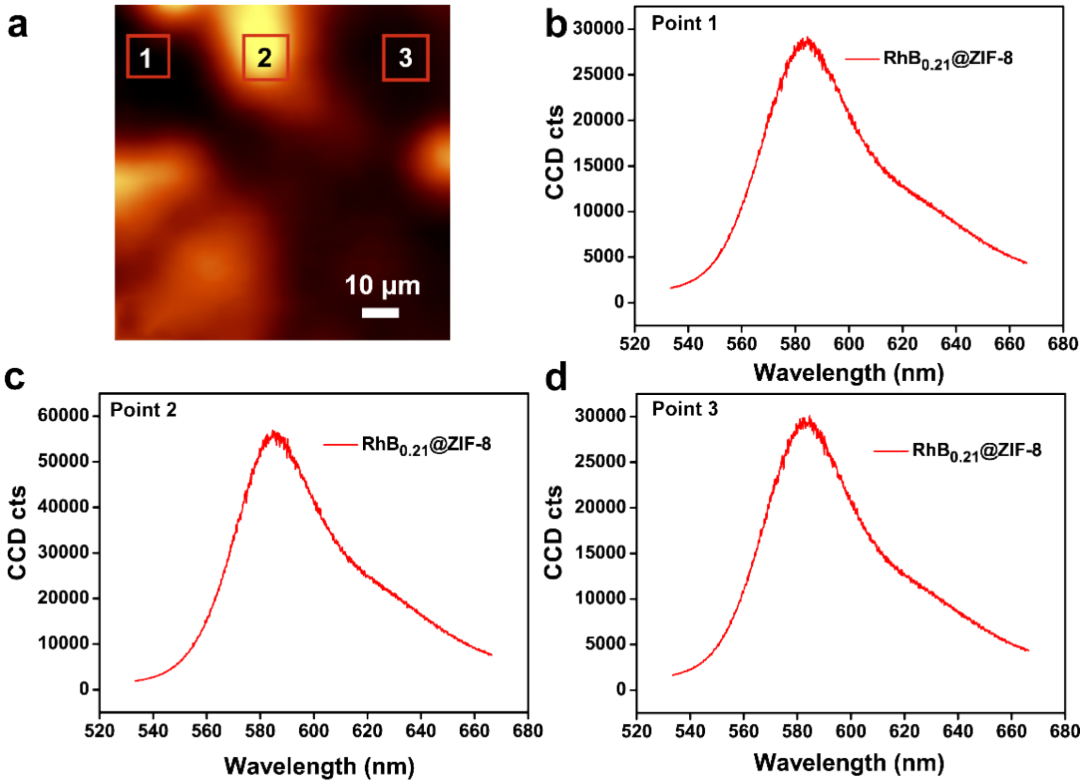

Fig. S11 (a) PL map of $RhB_{0.21}$@ZIF-8 excited by 488 nm; (b) PL spectra of point one on $RhB_{0.21}$@ZIF-8; (c) PL spectra of point two on $RhB_{0.21}$@ZIF-8; (d) PL spectra of point three on $RhB_{0.21}$@ZIF-8.

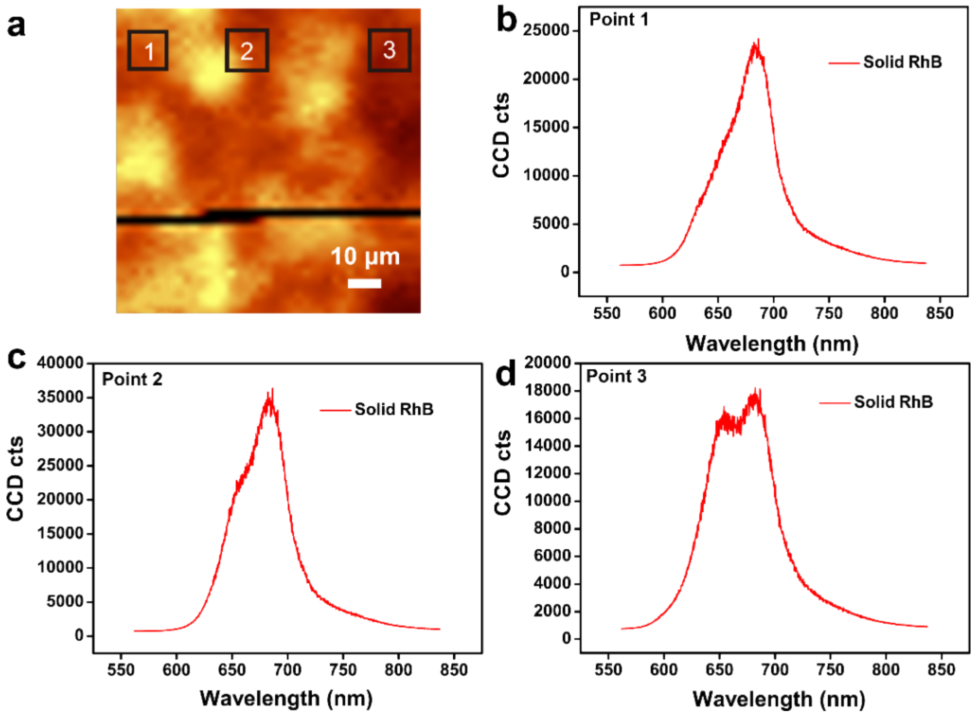

Fig. S12 (a) PL map of RhB excited by 488 nm; (b) PL spectra of point one on RhB; (c) PL spectra of point two on RhB; (d) PL spectra of point three on RhB.

After encapsulating the dye, it was investigated whether RhB@ZIF-8 can show uniformly emission properties. Photoluminescence (PL) mapping of $RhB_{0.21}$@ZIF-8 was conducted under 488 nm lasers excitation by Raman spectroscopy. Three different areas were chosen to prove the uniform emission of $RhB_{0.21}$@ZIF-8. All of the areas showed only one maximum emission peak (around 585 nm) (Fig. S11). In addition, the inner region looks much brighter than the edge region for each $RhB_{0.21}$@ZIF-8. For solid RhB, the emission peaks were not only one in different areas and ranged from 654 nm to 686 nm (Fig. S12). From above experiments, we concluded that $RhB_{0.21}$@ZIF-8 prepared by PISA showed only one aggregation state in solid states, which means pressure promotes the interaction between MOFs and dye molecules. In addition, the solvent ripening of MOFs enhanced the uniformly of dispersed dyes in MOF composites.

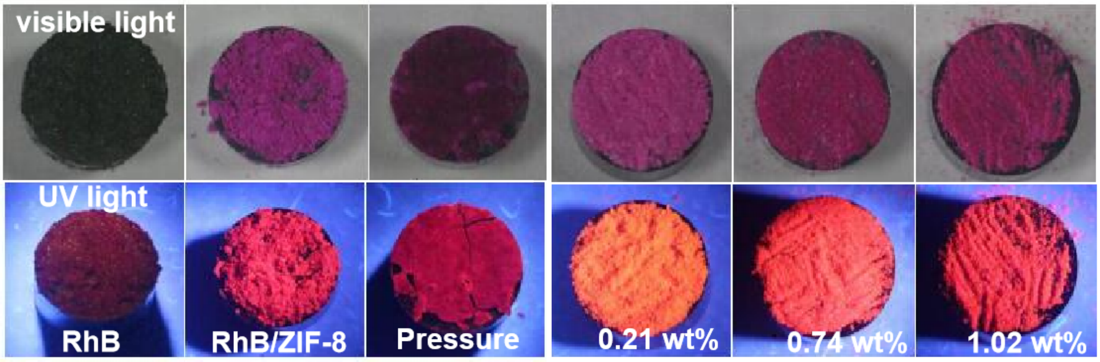

Fig. S13 Selected RhB_n@ZIF-8, RhB, mixed RhB/ZIF-8, pressed RhB/ZIF-8 viewed under room light and ultraviolet light (centered at 365 nm).

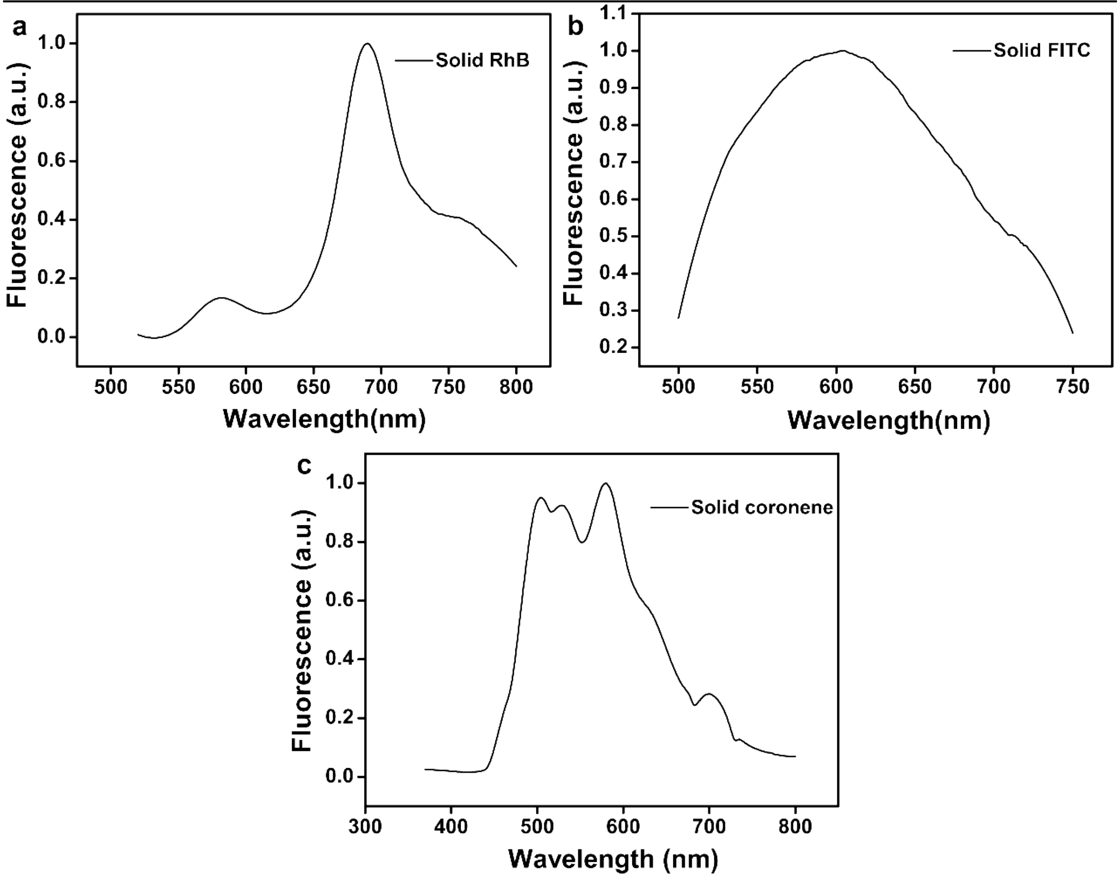

Fig. S14 Emission spectroscopy of solid RhB, solid FITC, and solid coronene.

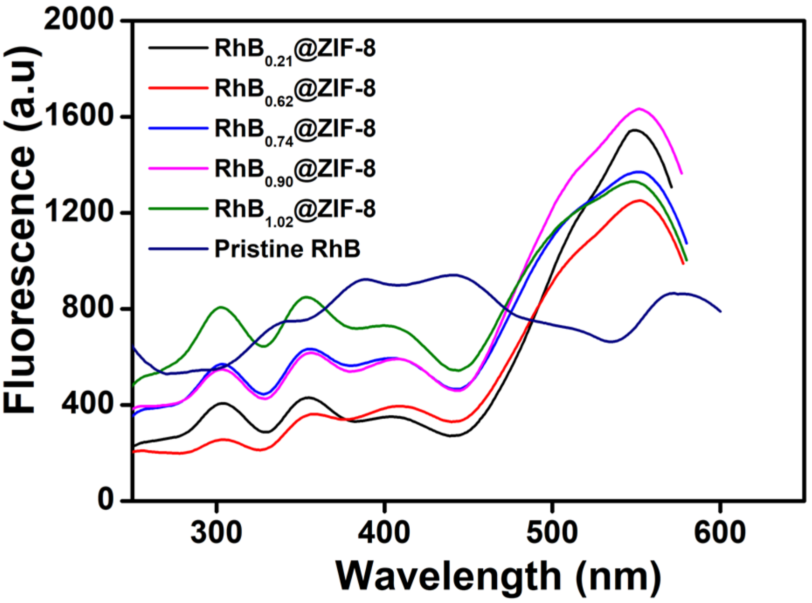

Fig. S15 Excitation spectroscopy of RhB$_n$@ZIF-8 and solid RhB. The maximum absorption wavelength for RhB$_n$@ZIF-8 was mainly in the range of 548 nm-551 nm. The maximum absorption wavelength for solid RhB is 388 nm-442 nm.

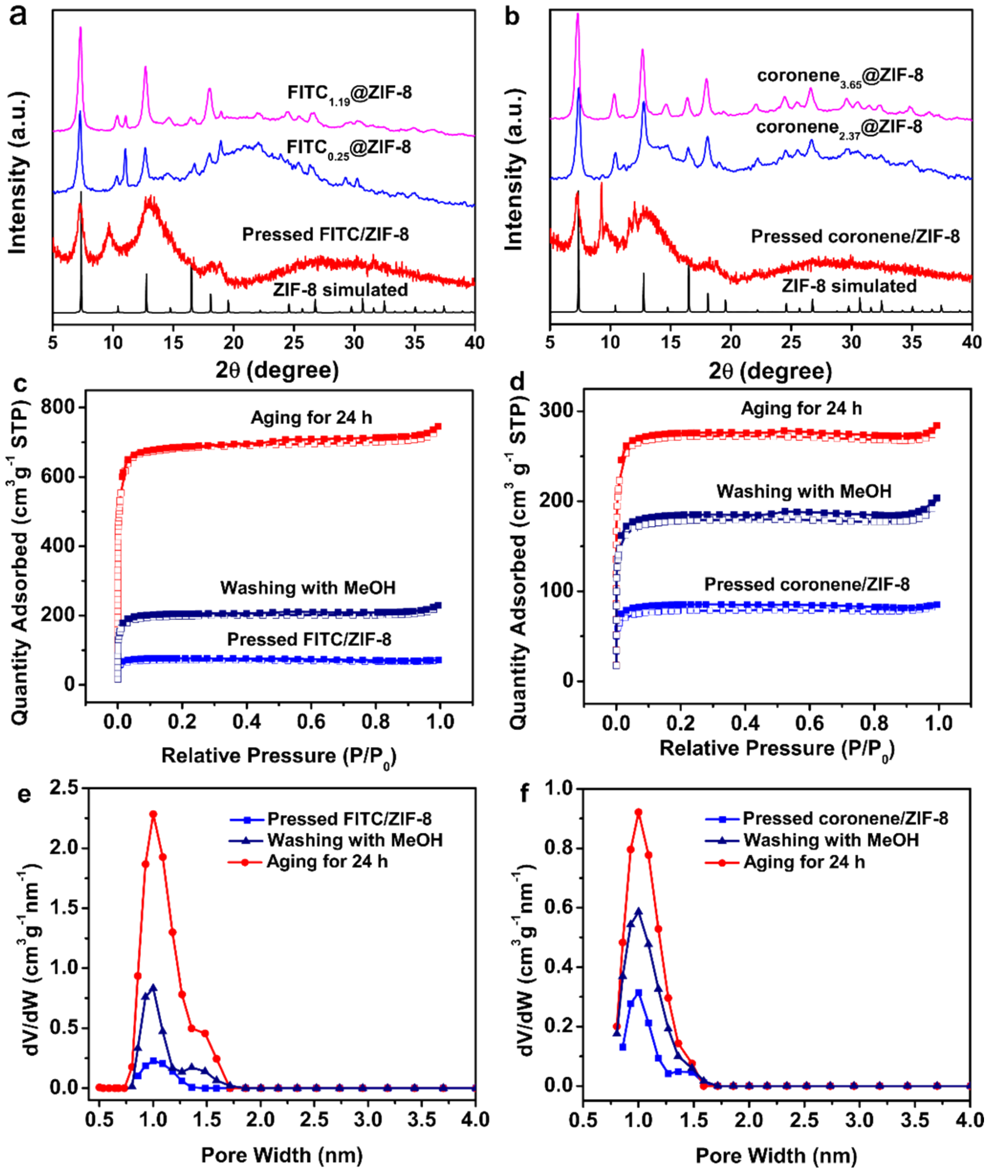

Fig. S16 (a) PXRD patterns of pressed FITC/ZIF-8, pressed FITC/ZIF-8 after MeOH aging and simulated for ZIF-8. (b) PXRD patterns for pressed coronene/ZIF-8, pressed coronene/ZIF-8 after MeOH aging and simulated for ZIF-8. (c) N_2 adsorption-desorption isotherms for pressed FITC/ZIF-8, pressed FITC/ZIF-8 after MeOH washing and pressed FITC/ZIF-8 after MeOH aging. (d) N_2 adsorption-desorption isotherms for pressed coronene/ZIF-8, pressed coronene/ZIF-8 after MeOH washing and pressed coronene/ZIF-8 after MeOH aging. (e) Pore size distributions of pressed FITC/ZIF-8, pressed FITC/ZIF-8 after MeOH washing and pressed FITC/ZIF-8 after MeOH aging. (f) Pore size distributions of pressed coronene/ZIF-8, pressed coronene/ZIF-8 after MeOH washing and pressed coronene/ZIF-8 after MeOH aging.

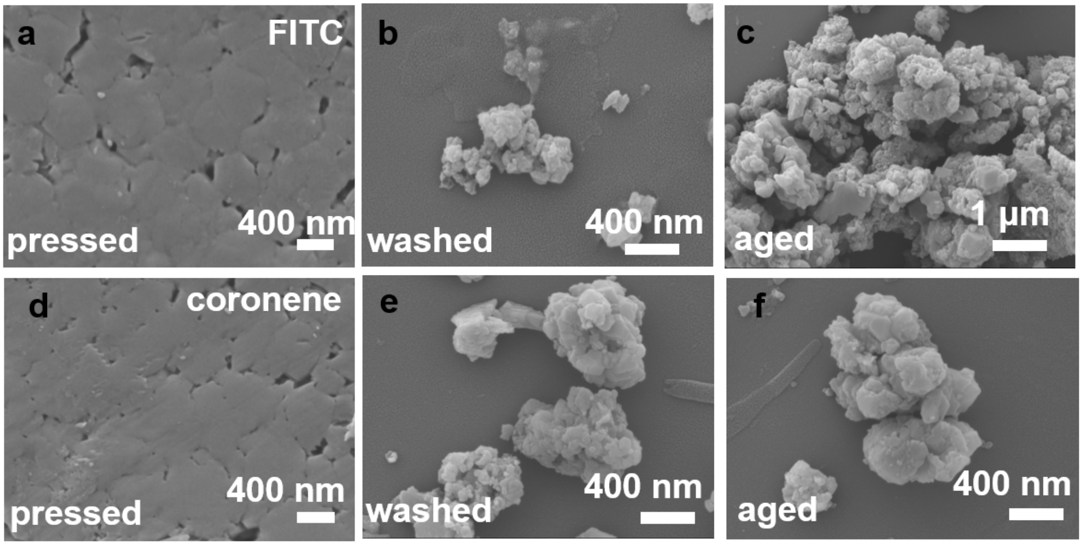

Fig. S17 (a) SEM images of pressed FITC/ZIF-8. (b) SEM images of pressed FITC/ZIF-8 after MeOH washing. (c) SEM images of pressed FITC/ZIF-8 aging in MeOH for 24 h. (d) SEM images of pressed coronene/ZIF-8. (e) SEM images of pressed coronene/ZIF-8 after MeOH washing. (f) SEM images of pressed coronene/ZIF-8 aging in MeOH for 24 h.

The phase transition process of FITC/ZIF-8 and coronene/ZIF-8 mixtures during pressing and MeOH aging were characterized by PXRD, SEM and N_2 adsorption-desorption, respectively. As shown in Fig. S16a-b, when the FITC/ZIF-8 and coronene/ZIF-8 were pressed, the broadening of the diffraction peaks and the decrease of intensity indicated that the crystallinity of ZIF-8 decreased and partially disordered structures appeared. After high pressure treatment, the specific surface area of FITC/ZIF-8 and coronene/ZIF-8 decreased directly to 281.9 and 307.0 $m^2 \cdot g^{-1}$, respectively, which further proved the amorphization of ZIF-8. In addition, the porosity also decreased to 0.22 and 0.31 $cm^3 \cdot g^{-1} \cdot nm^{-1}$ respectively due to pore collapse. From N2 sorption experiments, the specific surface area of direct washing increased (FITC/ZIF-8: 281.9 to 650.7 $m^2 \cdot g^{-1}$; coronene/ZIF-8: 307.0 to 610.0 $m^2 \cdot g^{-1}$), and the porosity increased (FITC/ZIF-8: 0.22 to 0.81 $cm^3 \cdot g^{-1} \cdot nm^{-1}$; coronene/ZIF-8: 0.31 to 0.58 $cm^3 \cdot g^{-1} \cdot nm^{-1}$), indicating that the partially amorphous ZIF-8 has been transformed into crystalline ZIF-8 after methanol washing. After 24 h recovery, the specific surface area of dyes/ZIF-8 was changed after washing: FITC@ZIF-8 is 2240.9 $m^2 \cdot g^{-1}$ and coronene@ZIF-8 was 974.2 $m^2 \cdot g^{-1}$. The SEM images further confirmed that high pressure can transform regular dodecahedron ZIF-8 particles into partially disordered assembled particles (Fig. S17). After washing with MeOH, the morphology of ZIF-8 in FITC/ZIF-8 and coronene/ZIF-8 were basically recovered.

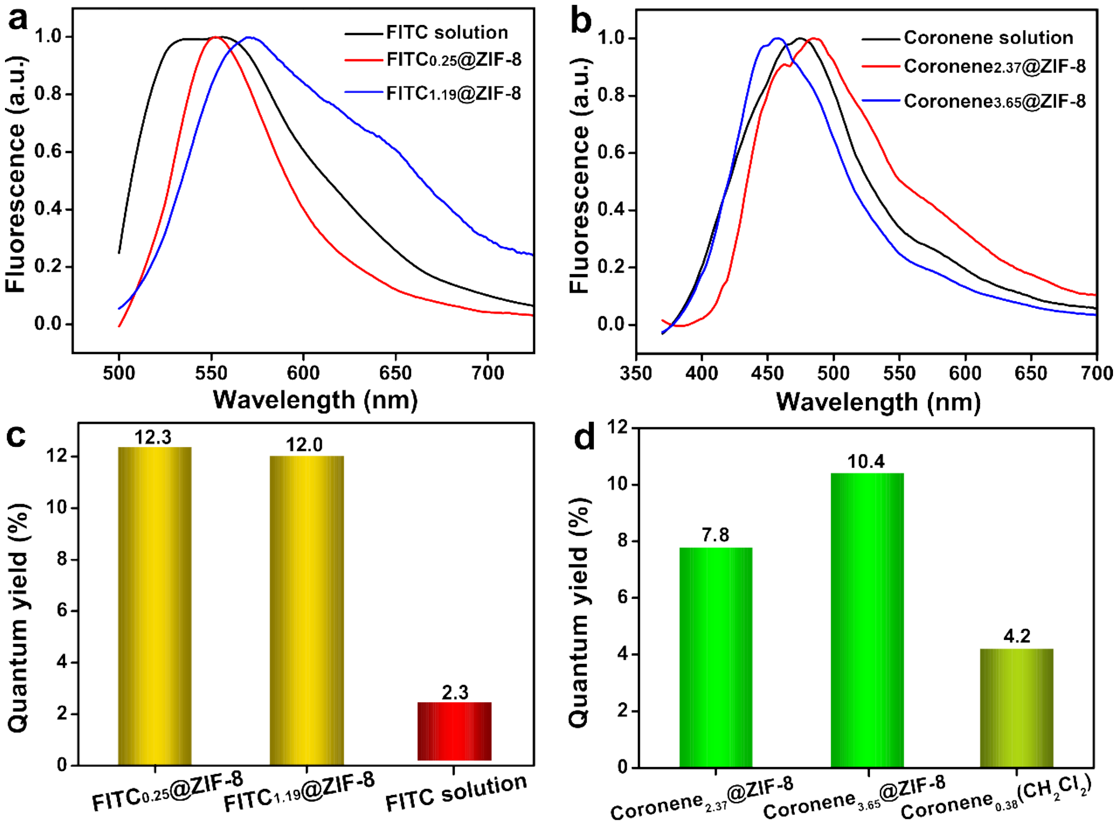

Fig. S18 (a) Emission spectra of FITC in DMSO solution and FITC@ZIF-8; (b) Emission spectra of coronene in CH_2Cl_2 solution and coronene@ZIF-8; (c) Quantum yield of FITC in DMSO and FITC@ZIF-8; (d) Quantum yield of coronene in CH_2Cl_2 and coronene@ZIF-8.

For ionic dyes such as FITC, which are often used to label enzymes and other biomolecules, the fluorescent spectrum of composite materials constructed by PISA compared to solid FITC has shifted from 603 nm to 552 nm with the 0.25 wt% loading of dyes, to the 571 nm with the 1.19 wt% loading of dyes. The quantum yield and lifetime of FITC@ZIF-8 were increased compared to solid FITC and FITC in DMSO (Table S3, S6). For rigid molecules such as coronene, the emission of dyes also had a blue shift compared with solid dyes, this is mainly due to the strong π-π stacking effect of coronene. Corenene@ZIF-8 showed increased quantum yield with the increasing of loading (Table S5, S6).

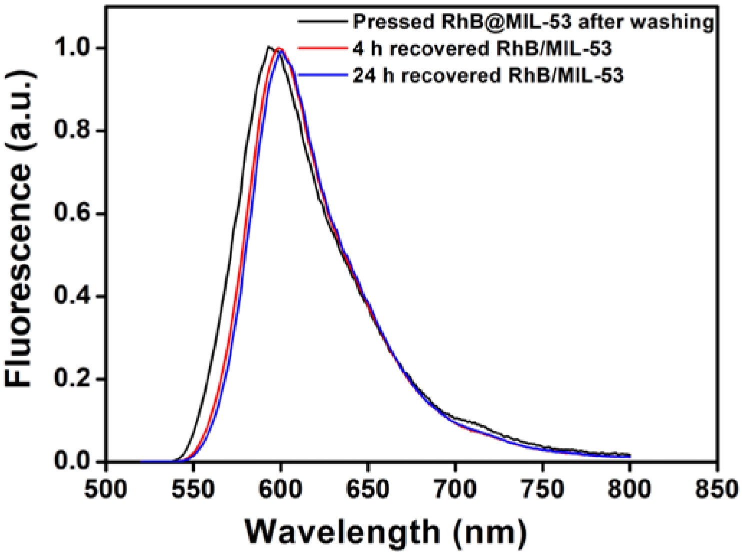

Fig. S19 The fluorescence emission spectra for RhB@MIL-53 after aging in MeOH for different time upon excitation at 500 nm.

References

1. H. N. Abdelhamid, Z. Huang, A. M. El-Zohry, H. Zheng and X. Zou, *Inorg. Chem.*, 2017, **56**, 9139-9146.
2. U. Resch-Genger, M. Grabolle, S. Cavaliere-Jaricot, R. Nitschke and T. Nann, *Nat. Methods*, 2008, **5**, 763-775.
3. L. Gong, Q. Zhang, L. Wang, J. Wu, C. Han, B. Lei, W. Chen, G. Eda, K. E. J. Goh and C. H. Sow, *Nano Res.*, 2018, **11**, 4574-4586.
4. R. Rao, V. Carozo, Y. Wang, A. E. Islam, N. Perea-Lopez, K. Fujisawa, V. H. Crespi, M. Terrones and B. Maruyama, *2D Mater.*, 2019, **6**, 045031.
5. V. Martinez, B. Karadeniz, N. Biliškov, I. Lončarić, S. Muratović, D. Žilić, S. M.

Avdoshenko, M. Roslova, A. A. Popov and K. Užarević, *Chem. Mater*, 2020, **32**, 10628-10640.

6. X.Y. Liu, K. Xing, Y. Li, C.K. Tsung and J. Li, *J. Am. Chem. Soc.*, 2019, **141**, 14807-14813.
7. Z. Wang, Z. Wang, B. Lin, X. Hu, Y. Wei, C. Zhang, B. An, C. Wang and W. Lin, *ACS Appl. Mater. Interfaces*, 2017, **9**, 35253-35259.
8. W. Chen, Y. Zhuang, L. Wang, Y. Lv, J. Liu, T.-L. Zhou and R.-J. Xie, *ACS Appl. Mater. Interfaces*, 2018, **10**, 18910-18917.
9. H. Mieno, R. Kabe, N. Notsuka, M. D. Allendorf and C. Adachi, *Adv. Opt. Mater.*, 2016, **4**, 1015-1021.
10. H. N. Abdelhamid, Z. Huang, A. M. El-Zohry, H. Zheng and X. Zou, *Inorg. Chem.*, 2017, **56**, 9139-9146.
11. H. H. Rao, Z. H. Xue, G. H. Zhao, S. Y. Li, X. Z. Du, *J. Non. Cryst. Solids.*, 2016, **450**, 32-37.